Advances in Energy Research, *Vol. 8, No. 4 (2022) 265-273*
https://doi.org/10.12989/eri.2022.8.4.265

Coal pyrolysis behaviors at supercritical CO_2 conditions

Hakduck Kim[1a], Jeongmin Choi[2b], Heechang Lim[2c] and Juhun Song*[2]

[1]*Graduate School of Convergence for Clean Energy Integrated Power Generation, Pusan National University, Republic of Korea*
[2]*School of Mechanical Engineering, Pusan National University, Republic of Korea*

(*Received May 15, 2021, Revised July 4, 2022, Accepted July 27, 2022*)

Abstract. In this study, a product gas yield and carbon conversion were measured during the coal pyrolysis. The pyrolysis process occurred under two different atmospheres such as subcritical (45 bar, 10ºC) and supercritical CO_2 condition (80 bar, 35ºC). Under the same pressure (80 bar), the atmosphere temperature increased from 35°C to 45°C to further examine temperature effect on the pyrolysis at supercritical CO_2 condition. For all three cases, a power input supplied to heating wire placed below coal bed was controlled to make coal bed temperature constant. The phase change of CO_2 atmosphere and subsequent pyrolysis behaviors of coal bed were observed using high-resolution camcorder. The pressure and temperature in the reactor were controlled by a CO_2 pump and heater. Then, the coal bed was heated by wire heater to proceed the pyrolysis under supercritical CO_2 condition.

Keywords: coal pyrolysis; phase change; product gas yield; P-T diagram; Supercritical CO_2 ($ScCO_2$)

1. Introduction

In our prior work (Kim and Song 2020), we investigated the coal gasification behavior at gaseous carbon dioxide (gCO_2) condition of 45 bar. This gasification occurred at the subcritical pressure which is lower than critical pressure (73 bar) and temperature (32°C). The extraction of supercritical CO_2 ($ScCO_2$) was widely used for drying (Song and Sun 2020, Iwai and Arai 1998) and cleaning application (Hariyanto and Kim 2020, Samanta and Ghosh 2015). Song and Sun (2020) observed a greater change of pore structure at supercritical CO_2 condition as compared to the subcritical state. These were attributed to higher wettability and resultant adsorption behavior of $ScCO_2$. Arai *et al.* (1998) observed much easier water drying of $ScCO_2$ for coals than water removal for a zeolite. The drying extent was different depending on coal types, which indicates interaction of $ScCO_2$ and water contained in the coal samples. Kim *et al*. (2020) used a $ScCO_2$ drying technique to completely remove ethanol from a biomass powder in shorter time than with oven drying process. Yurchick and Hill (2021) reported a supercritical treatment for coal to be converted to valuable products such as liquid and gases. Zhang and Tao (2013) demonstrated that

*Corresponding author, Ph.D., E-mail: jxs704@pusan.ac.kr
[a]E-mail: win200162@naver.com
[b]E-mail: jungmin911027@naver.com
[c]E-mail: hclim@pusan.ac.kr

http://www.techno-press.org/?journal=eri&subpage=7 ISSN: 2287-6316 (Print), 2287-6324 (Online)

Table 1 Power inputs required to heat the coal bed to the same temperature (700℃) at different CO_2 pressure conditions

Cases	Voltage (V)	Current (I)	Power (W)
Case 1 (45bar, 10℃)	2.3	6.5	14.9
Case 2 (80bar, 35℃)	3.5	9.0	31.5
Case 3 (80bar, 45℃)	3.0	8.3	24.9

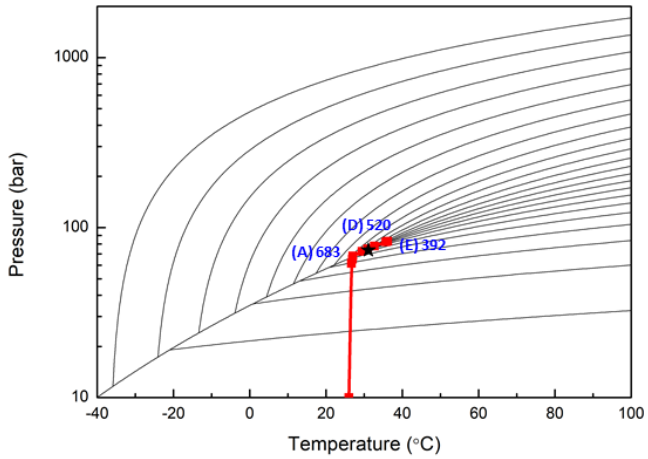

Fig. 1 The pressure-temperature (P-T) diagram of CO_2 measured in this experiment

$ScCO_2$ injection changes the microstructure of coal and extracts the hydrocarbons present in the coal matrix even at room temperature. Nonetheless, the effect of supercritical treatment of CO_2 on the volatile release from coal surface was not studied thoroughly. Therefore, coal pyrolysis and gasification behavior at supercritical CO_2 condition was examined in this study.

2. Experimental setup

In this study, a sub-bituminous coal was used. The coal contains high volatile and moisture content of about 40 and 20%, respectively. More descriptions about coal properties are found in previous publications (Kim and Song 2021, 2022). A wire heating was employed to heat the coal bed inside the crucible. The weight of coal bed was 40 mg. Using such small amount of coal did not affect the temperature and pressure of chamber when it was reacted during the gasification. The coal gasification was allowed to occur for 300 s. Power inputs required to heat the coal bed at different CO_2 pressure conditions are listed in Table 1. Power input was adjusted to make gasification occur at the same temperature (700°C). For example, about two times higher power (31.5 W) was required to heat coal samples for case 2 (80 bar, 35°C) as compared to one (14.9 W) for case 1 (45 bar, 10°C).

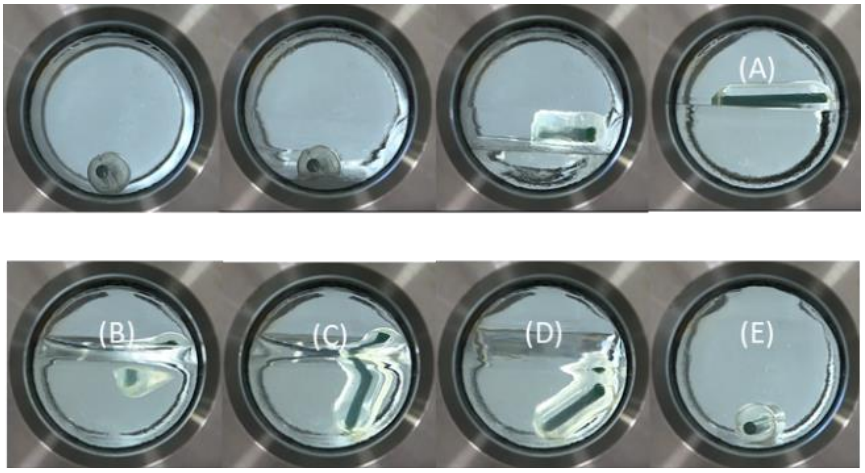

Fig. 2 The position of floating disk showing the density of CO_2 when it is pressurized and heated to supercritical CO_2 condition (case 2: 80 bar, 35°C)

The more details about reactor and heating methods can be found in the previous work of authors (Kim and Song 2021). Then, it was subsequently pyrolyzed and gasified under two CO_2 conditions. One is low CO_2 pressure (45 bar) which provides gaseous CO_2 at subcritical region. The other is high CO_2 pressure (80 bar), which goes above critical pressure (73 bar). In this way, the gasification occurs at supercritical CO_2 condition successfully.

Then, it was pyrolyzed and gasified under two CO_2 conditions. One is low CO_2 pressure (45 bar) which provides gaseous CO_2 at subcritical region. The other is high CO_2 pressure (83 bar), which goes above critical pressure (73 bar). In this way, the gasification occurs at supercritical CO_2 condition.

3. Results and discussion

3.1 Preparation of supercritical CO_2 condition

Fig. 1 presents the pressure-temperature (P-T) diagram of CO_2. The pressure increased from 1 to 80 bar at the room temperature (25°C) using the CO_2 pump. Then, the temperature slowly increased to 35°C in accordance with saturated line for this pure CO_2 substance. The reactor was wrapped with heating tape to increase the temperature. The pressure and temperature of CO_2 passed through the critical temperature (32°C) and pressure (73 bar). This critical point was marked by black asterisk in the P-T diagram of Fig. 1. The densities at different states (A-E) were calculated by using the REFPROP software (Lemmon 2007) and was listed in the P-T diagram. The density decreased from 683 kg/m^3 at state A (liquid state) to 392 kg/m^3 at state E (supercritical CO_2 state).

As shown in Fig. 2, a custom-made floating disk was used to visualize the density change of CO_2 fluid in the chamber. Once CO_2 density (state D) becomes smaller than density of the disk (450 kg/m^3), the disk completely falls down to the bottom of the chamber. This condition corresponds to state (E) in the image of Fig. 2.

3.2 Coal pyrolysis and gasification behavior at supercritical CO_2 condition

The product gas yield and carbon conversion were measured during the coal pyrolysis and gasification. The coal pyrolysis process occurred under two different atmospheres: subcritical (45 bar, 10ºC) and supercritical CO_2 condition (80 bar, 35ºC). These are denoted by gCO_2 and $ScCO_2$, respectively. The third condition was a supercritical condition with the same pressure and higher temperature (80 bar, 45ºC). The yield of a specific gas was calculated from the mass of product gas (m_i) as expressed in Eq. (1). This requires the knowledge about the specific volume of total gas (v_t).

$$m_i = x_i \cdot N_t \cdot MW_i = x_i \cdot \frac{V_t}{v_t MW_t} \cdot MW_i \tag{1}$$

where x_i is mole fraction of i[th] gas species, V_t is chamber volume filled with total gas, v_t is specific volume of total gas, MW_t is molecular weight of i[th] gas species.

There are three different methods to calculate the specific volume of total gas (v_t) required in Eq. (1). One is a direct use of property table incorporated in REFPROP software. The second and third method are using the Peng–Robinson equation of state (Eq. (2)) and van der Walls equation of state (Eq. (3)), respectively. The details about these equations of state (EoS) are extensively described in classical thermodynamics book of Cengel and Boles (2010) as well as Borgnakke and Sonntag (2014). Coefficients of a and b are determined using critical point temperature and pressures for CO_2.

$$P = \frac{RT}{(v-b)} - \frac{a \cdot \alpha}{v^2 + 2bv - b^2} \tag{2}$$

where $a = 0.45274 \cdot \frac{R^2 T_c^2}{P_c}$, $b = 0.07780 \cdot \frac{RT_c}{P_c}$,

$$\alpha = \left[(1 + (0.37464 + 1.54226\omega - 0.26992\omega^2)(1 - \sqrt{\frac{T}{T_c}}) \right]^2, \quad w = 0.225$$

$$P = \frac{RT}{(v-b)} - \frac{a}{v^2} \tag{3}$$

where $a = \frac{27R^2T_c^2}{64P_c}$, $b = \frac{RT_c}{8P_c}$,

The specific volume of total gas is calcuated from 1st method (property table) and listed in Table 2. This may be considered as exact solution. As the case changes from subcritical to supercritical, the specific volume decreases and then increases with further temperature increase at 80 bar. The pressure was calculated at various specific volumes from Peng–Robinson equation of state (2) and the resultant p-v diagram is plotted in Fig. 3. In similar way, P-v curves were obtained using van der Walls equation of state (3) and shown in Fig. 4. Both results of van der Walls and P-R equation produced 0.0024 and 0.004 for case 2 and case 3 near supercritical conditions. These values are consistent with those (0.0023, 0.0041) predicted from property table in Table 2. However, the van der Walls model did not even have a solution of a liquid volume for case 1 (45

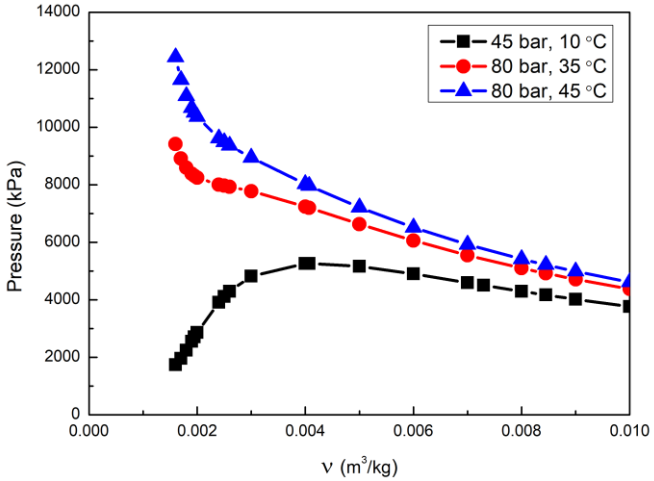

Fig. 3 The pressure-volume (P-v) diagram for three cases based on Peng Robinson equation of state (EoS)

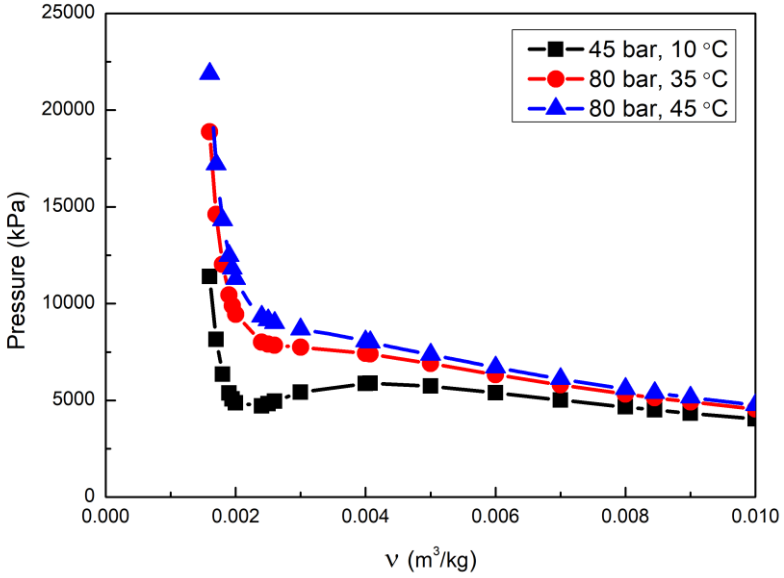

Fig. 4 The pressure-volume (P-v) diagram for three cases based on van der Walls equation of state (EoS)

bar, 10°C) at subcritical condition. Furthermore, it overpredicted a vapor volume (0.0085), which is higher than predicted from property table (0.0075). However, the Peng Robinson model predicted 0.0012 for liquid volume and 0.0075 for vapor volume, which are the same as those predicted from property table.

Table 2 Calculation of specific volume of total gas using the property table in REFPROP

Cases	Liquid volume, v_f (m^3/kg)	Vapor volume, v_g (m^3/kg)	P (kPa)
Case 1 (45 bar, 10 °C)	0.0012	0.0075	4500
Case 2 (80 bar, 35 °C)	NA	0.0023	8000
Case 3 (80 bar, 45 °C)	NA	0.0041	8000

Table 3 Variation of CO_2 properties with pressure and temperature

CO_2 conditions	Density (kg/m^3)	Specific heat capacity (kJ/kg-K)	Surface tension (mN/m)
Case 1 (45 bar, 10°C)	135	2.5	2.7
Case 2 (80 bar, 35°C)	436	33.3	N/A
Case 3 (80 bar, 45°C)	242	3.2	N/A

Figs. 5(a) and 5(b) presents CO and H_2 gas yield at different CO_2 pressures and temperatures. The carbon conversion data was also available in (c) of the figure. This was calculated based on mass change of coal bed. The results of the gasification showed 47% increase in CO yield and 300 % increase in H_2 yield at supercritical condition (case 2) as compared to one at subcritical CO_2 condition (case 1). Because of the presence of supercritical CO_2, the volatile and water can be released from the coal surface more easily. However, the carbon conversion remained nearly the same at 40% for three cases as shown in Fig. 5(c). The difference between a product yield sum of two light gases (CO, H_2) and carbon conversion would be due to liquid components such as heavy hydrocarbon called tar and condensed water. The liquid components ranged from 7% for case 2 in supercritical CO_2 condition to 20% for case 1 in subcritical CO_2 condition. This indicates that light gases such as CO and H_2 are more easily extracted than heavy volatile contents when a coal is treated by supercritical CO_2.

Fig. 6 shows visual observations at the onset of gasification at three different CO_2 conditions. The earliest volatile release is observed for case 2 with CO_2 pressure (80 bar/35°C). The cloud made of light gases begins to appear significantly at 0.15 s for case 2 in supercritical CO_2 condition. In contrast, the clouds were not observed for case 1 in subcritical CO_2 condition at the same time (0.15 s) and even later (1 s). This is consistent with highest CO yield observed from product gas measurement previously reported for case 2.

3.3 Effect of CO_2 temperature on supercritical coal gasification behavior

As shown in Fig. 5(a), CO yield decreased when the CO_2 temperature further increased from 35 to 45°C. The variation in some properties of CO_2 with pressure and temperature are calculated from the REFPROP software and listed in Table 3. As inferred from the density data, the density decreased from 436 to 242 kg/m^3. The decrease in CO yield can be attributed to such reduction in density which may weaken the impact of supercritical CO_2 treatment. In contrast, further temperature continuously increased the H_2 gas yield from 0.3 to 0.42%, which are substantially smaller than CO gas yield (20-30%). This is different from the CO yield observed with temperature increase as described earlier.

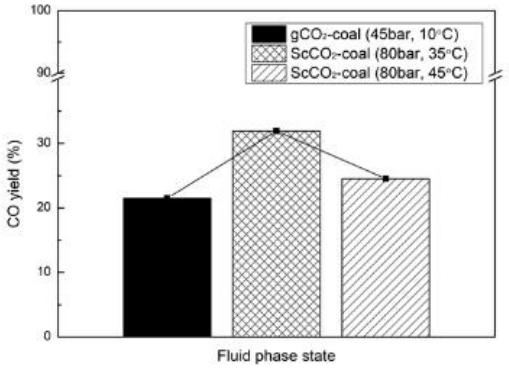

(a)

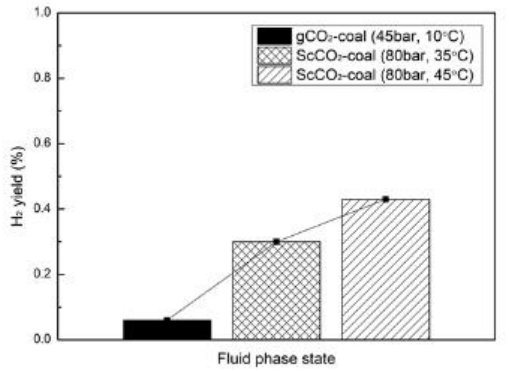

(b)

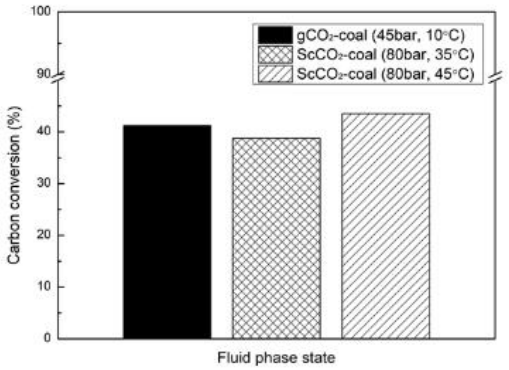

(c)

Fig. 5 (a) CO gas yield, (b) H_2 gas yield and (c) carbon conversion produced from coal gasification at different CO_2 pressures and temperatures

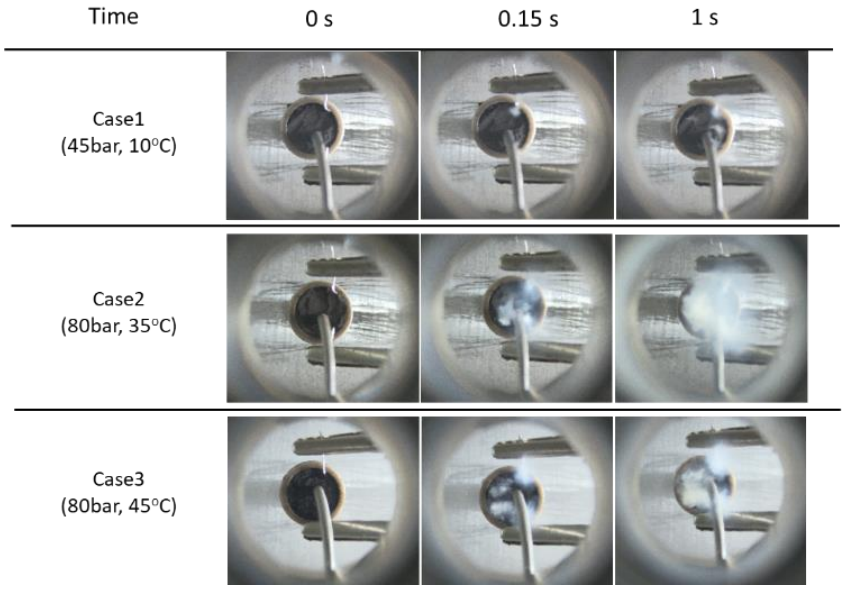

Fig. 6 Visualization of coal gasification process at three different CO_2 conditions

4. Conclusions

In this study, a product gas yield and carbon conversion were measured during the coal pyrolysis and gasification. The coal gasification process occurred under two different atmospheres such as subcritical (45 bar, 10°C) and supercritical CO_2 condition (80 bar, 35°C). Under the same pressure (80 bar), the temperature of CO_2 atmosphere further increased to 45°C to examine the temperature effect on gasification at supercritical CO_2 condition. For all three cases, a power input supplied to heating wire below coal bed was controlled to make coal bed temperature constant (700°C).

The results showed 47% increase in CO yield and 300% increase in H_2 yield for the gasification at supercritical condition (case 2) as compared to one at subcritical CO_2 condition (case 1). Under the supercritical condition, further increase in temperature (case 3) leads to a reduction in the CO and a further increase in the H_2 yield. This indicates the higher light volatile and water release from the coal surface at supercritical CO_2 condition. However, the carbon conversion remained nearly the same for three cases.

Acknowledgments

This work was supported by Korea Institute of Energy Technology Evaluation and Planning (KETEP) grant funded by the Korea government (MOTIE) (20214000000140, Graduate School of Convergence for Clean Energy Integrated Power Generation). The authors also thank for the financial support from the National Research Foundation of Korea (NRF) grant (NRF-2020R1F1A1051343) funded by the Korean Government (MEST).

References

Borgnakke, C. and Sonntag, R.E. (2014), *Fundamentals of thermodynamics*, John Wiley & Sons.

Cengel, Y.A., Boles, M.A. and Kanoglu, M. (2010), *Thermodynamics: an engineering approach*, McGraw Hill

Charles Hill and Chris Yurchick (2021), "Coal to carbon fiber – Novel supercritical CO_2 solvated process", presented at 2021 NETL Annual Coal Processing Project Review Meeting.

Hariyanto, P., Myint, A.A. and Kim, J.H. (2020), "Ultrafast and complete drying of ecamsule solution using supercritical carbon dioxide with fluctuating pressure technique", *J. Supercrit. Fluid.*, **160**, 104795. https://doi.org/10.1016/j.supflu.2020.104795.

Iwai, Y., Amiya, M., Murozono, T. and Arai, Y. (1998), "Drying of coals by using supercritical carbon dioxide", *Ind. Eng. Chem. Res.*, **37**, 2893-2896. https://doi.org/10.1021/ie9709493.

Kim, H.D., Choi, J.M., Lim, H.C. and Song, J.H. (2021), "Enhanced combustion processes of liquid carbon dioxide (LCO2)–low rank coal slurry at high pressures", *Energy*, **237**, 121566 .https://doi.org/10.1016/j.energy.2021.121566.

Kim, H.D., Choi, J.M., Lim, H.C. and Song, J.H. (2022), "Liquid carbon dioxide drying and combustion behavior of high-moisture coal at high pressure", *Appl. Therm. Eng*., **207**, 118182. https://doi.org/10.1016/j.applthermaleng.2022.118182.

Kim, H.D., Lim, H.C. and Song, J.H. (2020), "Effect of liquid carbon dioxide on coal pyrolysis and gasification behavior at subcritical pressure conditions", *Chem. Eng. Sci.*, **231**, 116292. https://doi.org/10.1016/j.ces.2020.116292.

Lemmon, E., Huber, M.L. and McLinden, M.O. (2007), *NIST Standard reference database 23*, Reference fluid thermodynamic and transport properties - REFPROP, Version 8.0.

Samanta, S. and Ghosh, S. (2015), "A techno-economic analysis of partial repowering of a 210 MW coal fired power plant", *Adv. Energ. Res.*, **3**, 167-179. https://doi.org/10.12989/eri.2015.3.3.167.

Song, Y., Zou, Q., Su, E., Zhang, Y. and Sun, Y. (2020), "Changes in the microstructure of low-rank coal after supercritical CO2 and water treatment", *Fuel,* **279**, 118493. https://doi.org/10.1016/j.fuel.2020.118493.

Zhang, D., Gu, L., Li, S., Lian, P. and Tao, J. (2013), "Interactions of Supercritical CO_2 with Coal", *Energ. Fuel.*, **27,** 387-393. https://doi.org/10.1021/ef301191p.